

# Anisotropic scaling in braided rivers: An integrated theoretical framework and results from application to an experimental river

Efi Foufoula-Georgiou and Victor B. Sapozhnikov

St. Anthony Falls Laboratory, University of Minnesota, Minneapolis

**Abstract.** Dynamic scaling in braided rivers is reexamined under an extended theoretical framework, developed herein, which explicitly incorporates the self-affinity (scaling anisotropy) in the spatial structure of braided rivers. It is shown that in structures exhibiting anisotropic spatial scaling, dynamic scaling (if present) is necessarily anisotropic. Through analysis of the behavior of an experimental braided river, the presence of anisotropic dynamic scaling in braided rivers was revealed. This implies that there exists a pair of dynamic exponents  $z_x$  and  $z_y$  enabling one to rescale space (differently in the direction  $X$  of the slope and in the perpendicular direction  $Y$ ) and time, such that the evolution of a smaller part of a braided river looks statistically identical to that of a larger one. The presence of such a space-time scale invariance provides an integrated framework for describing simultaneously the spatial and temporal structure of braided rivers and may be explored toward statistical prediction of large and rare changes from the statistics of smaller and frequent ones.

## 1. Introduction

The morphology and dynamics of braided rivers have been studied over the years using river-mechanics, experimental, empirical, and computer-simulation approaches [e.g., see Howard *et al.*, 1970; Schumm and Khan, 1972; Ashmore, 1982, 1991; Kuhnle, 1981; Leddy *et al.*, 1993; Barzini and Ball, 1993; Murray and Paola, 1994; Smith *et al.*, 1995, 1996]. In a recent study, Sapozhnikov and Foufoula-Georgiou [1997] analyzed the spatio-temporal structure of braided rivers and presented evidence that they exhibit dynamic scaling. Dynamic scaling implies that a small part of a braided river evolves identically (in a statistical sense) to a larger one provided that time is renormalized by a factor depending only on the ratio of the spatial scales of those parts. In those developments, Sapozhnikov and Foufoula-Georgiou [1997] considered braided rivers as self-similar objects characterized by one fractal dimension  $D$ . However, it is known [Sapozhnikov and Foufoula-Georgiou, 1996] that braided rivers exhibit spatial scaling anisotropy, i.e., are objects characterized by two scaling exponents  $\nu_x$  and  $\nu_y$ , or equivalently two fractal dimensions  $D_G$  and  $D_L$  (see Sapozhnikov and Foufoula-Georgiou [1995] for relations between  $D_G$ ,  $D_L$ , and  $\nu_x$ ,  $\nu_y$ ). The reason that self-similarity was assumed in the dynamic scaling developments of Sapozhnikov and Foufoula-Georgiou [1997] was that no theoretical framework existed yet to integrate the notions of dynamic scaling and self-affinity.

The scope of this paper is to present such a framework, i.e., extend the theory of dynamic scaling to self-affine objects, and report the results of reanalyzing braided rivers under this integrated and more consistent framework. To avoid repetition, relies heavily on the paper of Sapozhnikov and Foufoula-Georgiou [1997] for the basic ideas on dynamic scaling and the

Copyright 1998 by the American Geophysical Union.

Paper number 98WR00216.  
0043-1397/98/98WR-00216\$09.00

details of the experimental setting. The reader is advised to read the present paper in conjunction with the previous one for a complete understanding of this work.

## 2. Dynamic Scaling in Self-Affine Objects

The idea of dynamic scaling in a self-affine object can be qualitatively presented as follows. Suppose there is a self-affine object characterized by fractal exponents  $\nu_x$  and  $\nu_y$ , which evolves in time (such that its fractal characteristics are preserved at all times). The self-affinity (anisotropic spatial scaling) of the object implies that if one takes a picture of a part of the object of size  $X_1 \times Y_1$ , and a picture of a part of the same object of size  $X_2 \times Y_2$ , such that

$$\left(\frac{X_2}{X_1}\right)^{1/\nu_x} = \left(\frac{Y_2}{Y_1}\right)^{1/\nu_y}, \quad (1)$$

and projects these two parts onto two screens of the same size, (this would require different stretching of each image in  $X$  and  $Y$  directions) the images on the screens will be statistically indistinguishable. Suppose now that one makes another step and, instead of taking still pictures, videotapes the two regions and observes the evolution of the images on the two screens. In contrast to the still pictures, the movies will not be statistically indistinguishable. The rate of evolution will be different (slower for the larger scale). If, however, there exists a pair of dynamic exponents  $z_x$  and  $z_y$  such that for every  $X_1$ ,  $Y_1$  and  $X_2$ ,  $Y_2$  satisfying (1) it is possible to rescale the time as

$$\frac{t_2}{t_1} = \left(\frac{X_2}{X_1}\right)^{z_x} = \left(\frac{Y_2}{Y_1}\right)^{z_y}, \quad (2)$$

or, in other words, to play the movies at different speeds, such that the rate of the evolution is the same on both screens, then we say that in addition to static (spatial) scaling the system also shows dynamic scaling. Comparison of (1) and (2) bounds the values of the fractal exponents  $\nu_x$ ,  $\nu_y$ , and the dynamic exponents  $z_x$ ,  $z_y$  by

$$\frac{z_x}{z_y} = \frac{\nu_y}{\nu_x} \tag{3}$$

Thus we see that dynamic scaling in self-affine objects is necessarily anisotropic.

Following the developments of *Sapozhnikov and Foufoula-Georgiou* [1997], let us characterize the evolution of a fractal stationary object by “changes” in its pattern, where changes are defined as parts of the space which were not occupied by the object at a certain moment of time but became occupied after some time lag  $t$ . Although changes in a river are three-dimensional, as is the river itself, we only considered in our previous work and here their horizontal projections. Thus changes in a braided river reflect parts of the river where water depth changed (including dry areas which became covered with water and water-covered areas which became exposed). Let  $n(X, Y, x, y, t)$  denote the number of changes exceeding size  $x$  in the  $X$  direction and size  $y$  in the  $Y$  direction after some time lag  $t$  in a region of size  $X \times Y$ . Because the object is stationary and fractal, with constant fractal exponents  $\nu_x$  and  $\nu_y$ , the number of changes scales with the size of the observed region (see Appendix in *Sapozhnikov and Foufoula-Georgiou* [1997]) as

$$\begin{aligned} n(X_2, Y_2, x_1, y_1, t_1) &= n(X_1, Y_1, x_1, y_1, t_1) \left(\frac{X_2}{X_1}\right)^{1/\nu_x} \\ &= n(X_1, Y_1, x_1, y_1, t_1) \left(\frac{Y_2}{Y_1}\right)^{1/\nu_y} \end{aligned} \tag{4}$$

provided that (1) holds.

The presence of dynamic scaling, implying the same rate of evolution after rescaling space and time according to (2), means that if (2) and (1) hold, the number of changes exceeding the same relative size  $x \times y$  such that

$$\frac{x_1}{x_2} = \frac{X_1}{X_2}, \quad \frac{y_1}{y_2} = \frac{Y_1}{Y_2} \tag{5}$$

is the same on both screens, i.e.,

$$n(X_1, Y_1, x_1, y_1, t_1) = n(X_2, Y_2, x_2, y_2, t_2) \tag{6}$$

Suppose now that we fix the scale of the region of interest to  $X_2 \times Y_2$  and instead of zooming to different scales we follow the distribution of changes in this region as the object evolves. From (6) and (4) we obtain for the distribution of changes in the region  $X_2 \times Y_2$

$$\begin{aligned} n(X_2, Y_2, x_2, y_2, t_2) &= n(X_2, Y_2, x_1, y_1, t_1) \left(\frac{X_1}{X_2}\right)^{1/\nu_x} \\ &= n(X_2, Y_2, x_1, y_1, t_1) \left(\frac{Y_1}{Y_2}\right)^{1/\nu_y} \end{aligned} \tag{7}$$

provided that (1) and (2) hold. The variables  $X_2$  and  $Y_2$  are the same in both sides of (7) and therefore can now be dropped. Replacing  $X_1/X_2$  by  $x_1/x_2$  and  $Y_1/Y_2$  by  $y_1/y_2$  from (5) yields

$$x_1^{1/\nu_x} n(x_1, y_1, t_1) = x_2^{1/\nu_x} n(x_2, y_2, t_2) \tag{8}$$

$$y_1^{1/\nu_y} n(x_1, y_1, t_1) = y_2^{1/\nu_y} n(x_2, y_2, t_2). \tag{9}$$

Finally, we obtain the condition for the distribution of changes in a system showing dynamic scaling: there exists a pair of dynamic exponents  $z_x$  and  $z_y$  (bound by (3)) such that if (2) is true, i.e.,  $t/X^{z_x} = \text{const}$  and  $t/Y^{z_y} = \text{const}$  (which according to

(5) also implies  $t/x^{z_x} = \text{const}$  and  $t/y^{z_y} = \text{const}$ ), then  $x^{1/\nu_x} n(x, y, t) = \text{const}$  and  $y^{1/\nu_y} n(x, y, t) = \text{const}$ , or in other words the distribution of changes in such systems can be expressed as

$$n(x, y, t) = x^{-1/\nu_x} g_x\left(\frac{t}{x^{z_x}}, \frac{t}{y^{z_y}}\right) = y^{-1/\nu_y} g_y\left(\frac{t}{x^{z_x}}, \frac{t}{y^{z_y}}\right), \tag{10}$$

where  $g_x(\cdot)$  and  $g_y(\cdot)$  are some functions.

The two conditions:  $t/x^{z_x} = \text{const}$  and  $t/y^{z_y} = \text{const}$ , can be presented as  $t/x^{z_x} = \text{const}$  and  $x^{z_x}/y^{z_y} = \text{const}$ . With (3) the second condition can be rewritten as  $x^{1/\nu_x}/y^{1/\nu_y} = \text{const}$  and (10) can be rewritten as

$$n(x, y, t) = x^{-1/\nu_x} h_x\left(\frac{t}{x^{z_x}}, \frac{y^{1/\nu_y}}{x^{1/\nu_x}}\right) = y^{-1/\nu_y} h_y\left(\frac{t}{y^{z_y}}, \frac{x^{1/\nu_x}}{y^{1/\nu_y}}\right). \tag{11}$$

Note that (10) and (11) are equivalent to each other.

Since  $n(x, y, t)$  is a joint probability of exceedance, the distribution  $n(x, t)$  for all possible values of  $y$ , is  $n(x, t) \equiv n(x, 0, t)$ . Therefore from (11) we obtain

$$n(x' > x, t) \equiv n(x, t) = x^{-1/\nu_x} h_x\left(\frac{t}{x^{z_x}}, 0\right) = x^{-1/\nu_x} f_x\left(\frac{t}{x^{z_x}}\right). \tag{12}$$

Similarly,

$$n(y' > y, t) \equiv n(y, t) = y^{-1/\nu_y} f_y\left(\frac{t}{y^{z_y}}\right). \tag{13}$$

Note that  $n(x' > x, t)$  is the number of changes of size greater than  $x$  in the  $X$  direction (and having any size in the  $Y$  direction) and  $n(y' > y, t)$  has similar meaning for the  $Y$  direction. Equations (12) and (13) are the equations of dynamic scaling of a self-affine object. They imply that if a self-affine object of scaling exponents  $\nu_x$  and  $\nu_y$  exhibits dynamic scaling, then there exist exponents  $z_x$  and  $z_y$  such that  $n(x' > x, t)x^{1/\nu_x}$  versus  $t/x^{z_x}$  and  $n(y' > y, t)y^{1/\nu_y}$  versus  $t/y^{z_y}$  collapse to the same curves  $f_x$  and  $f_y$ , respectively, for all  $x, y, t$ .

### 3. Analysis of an Experimental Braided River

Recognizing the lack of data for studying the evolution of natural braided rivers, *Sapozhnikov and Foufoula-Georgiou* [1997] proposed as a starting point to analyze the evolution of experimental braided rivers so that theories can be developed and tested until more accurate and frequent remote sensing data are available for application of these theories to natural systems. Thus, a small experimental basin of  $5 \text{ m} \times 0.75 \text{ m}$  was established at the St. Anthony Falls Laboratory and experimental braided rivers were successfully produced and monitored over time. The details of the experimental and monitoring procedures were extensively discussed by *Sapozhnikov and Foufoula-Georgiou* [1997] and are not repeated here. The same data of “changes” as in our previous paper are used here but subject to analysis under the extended theory of anisotropic dynamic scaling as developed in the previous section. For example, from the monitored changes over time the probabilities of exceedance  $n(x' > x, t)$  and  $n(y' > y, t)$  as needed in (12) and (13) were estimated now instead of the probability  $n(l' > l, t)$ ,  $l = \sqrt{\text{area}}$  used in the self-similar dynamic scaling analysis. The  $X$  direction is the direction of the slope and  $Y$  is the perpendicular direction.

It is noted that in principle, if the self-affine exponents  $\nu_x$  and  $\nu_y$  could be estimated directly from the river pattern using for example, the Logarithmic Correlation Integral (LCI)

method developed by the authors earlier [Sapozhnikov and Foufoula-Georgiou, 1995], then the dynamic exponents  $z_x$  and  $z_y$  could be estimated from (12) and (13) directly. That is, by nonlinear optimization the value of  $z_x$  that minimizes the spread of the points  $n(x' > x, t)x^{1/\nu_x}$  versus  $t/x^{z_x}$  (so that all curves collapse to a single curve  $f_x$ ) can be found. The  $z_y$  exponent could be found in the same way. However, as in the self-similar analysis we preferred to take advantage of a step-wise estimation approach suggested by the data. An additional reason for taking such an approach in the self-affine case is that  $\nu_x$  and  $\nu_y$  presented difficulty in their direct estimation from the experimental rivers because it was hard to separate the river from the colored sediment in the video images (dye was introduced in the water to monitor the evolution of the river). Therefore thus tracings of the river patterns could not reveal small channels thus restricting the range of analyzed scales. Note that determining the changes in the river pattern was not a problem because the colored sediment was zeroed by subtraction (see Sapozhnikov and Foufoula-Georgiou [1997] for details).

Changes in the experimental braided rivers, e.g., see Figure 2 of Sapozhnikov and Foufoula-Georgiou [1997], were followed over time and the sizes  $x$  and  $y$  of each change in the direction  $X$  of the slope and in the perpendicular direction  $Y$  were estimated as the root-mean square of the deviation of pixels  $(x_i, y_i)$  constituting the change, from the center of mass of the change  $(x_c, y_c)$ :  $x = [1/N \sum_{i=1}^N (x_c - x_i)^2]^{1/2}$  and  $y = [1/N \sum_{i=1}^N (y_c - y_i)^2]^{1/2}$ , correspondingly, where  $N$  is the number of the pixels in the change. Then cumulative probability distributions of the sizes  $x$  and  $y$  of changes were estimated. The distribution of changes was followed over time and Figure 1 shows these distributions for time lags of 3, 4, 5, 7, 9 and 15 s. Notice that the number of changes of size greater than  $x$  or  $y$  in a time lag  $t$ ,  $n(x' > x, t)$  and  $n(y' > y, t)$ , respectively, are plotted instead of the probability. As can be seen from Figure 1, these distributions can be well approximated by power laws for different time lags and the slopes of the log-log plots of the distributions found for different time lags are very close. Thus the distributions can be presented in the form

$$n(x' > x, t) = \psi_x(t)x^{-k_x}, \quad (14)$$

$$n(y' > y, t) = \psi_y(t)y^{-k_y}, \quad (15)$$

where  $\psi_x(t)$  and  $\psi_y(t)$  are functions of time lag  $t$ . The log-log plots of  $n(x' > x, t)x^{k_x}$  and  $n(y' > y, t)y^{k_y}$  against  $t$  shown in Figure 2 suggest that for small values of  $t$ ,  $\psi_x(t)$  and  $\psi_y(t)$  show power law dependencies

$$\psi_x(t) \sim t^{\beta_x} \quad (16)$$

$$\psi_y(t) \sim t^{\beta_y}. \quad (17)$$

Combining (14) and (16), and (15) and (17) we see that

$$n(x' > x, t) \sim t^{\beta_x}x^{-k_x} \quad (18)$$

$$n(y' > y, t) \sim t^{\beta_y}y^{-k_y}. \quad (19)$$

For small values of  $t$ , such that the power law relationships (16) and (17) hold, the functions  $f_x$  and  $f_y$  can be approximated by power laws. Thus, comparing the conditions of dynamic scaling (12) and (13) with (18) and (19), results in

$$z_x = (k_x - 1/\nu_x)/\beta_x \quad (20)$$

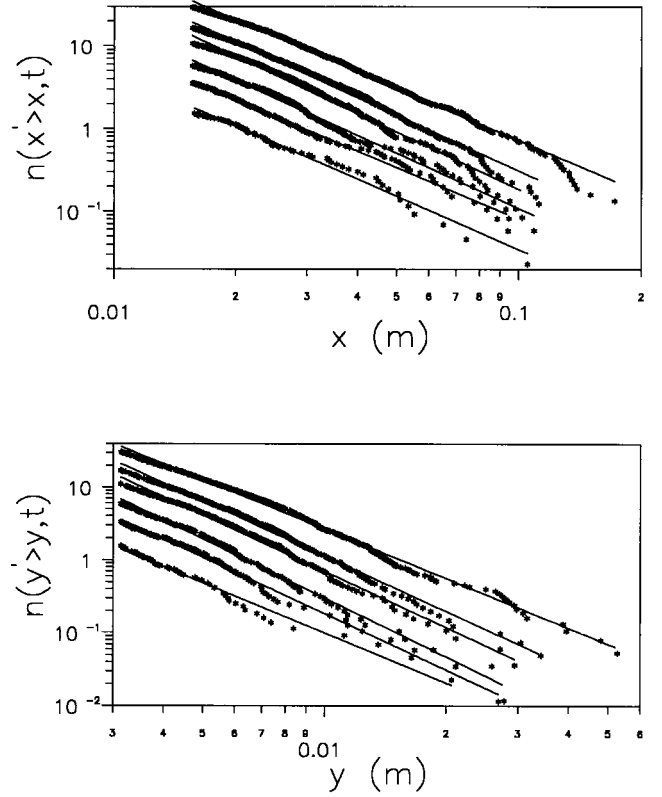


**Figure 1.** Number of changes of size greater than  $x$ ,  $n(x' > x, t)$ , and greater than  $y$ ,  $n(y' > y, t)$ , in the direction of slope  $X$  and the perpendicular direction  $Y$ , respectively. The numbers of changes are plotted for time lags  $t$  of 3, 4, 5, 7, 9, and 15 s (from bottom to top), and the solid lines represent the best least squares fit lines for each time lag  $t$ . Note that the numbers of changes are fractional numbers, some less than one, since they represent average values over multiple realizations, each realization corresponding to a particular time lag but to different time instances. The plots suggest that the distributions have broad central regions that are well approximated by power laws, and their slopes for different time lags are very close to each other for each of the two directions.

$$z_y = (k_y - 1/\nu_y)/\beta_y. \quad (21)$$

We estimated the values of  $k_x$  and  $k_y$  from the power-law distributions of changes (Figure 1 and (14) and (15)) as  $k_x = 2.17$  and  $k_y = 2.47$  ( $k_x$  and  $k_y$  represent the average of the slopes of the corresponding five lines in Figure 1). The values of  $\beta_x$  and  $\beta_y$  were estimated from the power law dependence of  $\psi_x(t)$  and  $\psi_y(t)$  (Figure 2 and (16) and (17)) as  $\beta_x = 1.68$  and  $\beta_y = 1.95$ .

As mentioned before, our experimental data did not permit a direct estimation of  $\nu_x$  and  $\nu_y$  via the LCI method. However, we were able to estimate the fractal dimension of the experimental braided river  $D$  from one pattern of the river by the “mass-in-a-box” method (which is much less data demanding) as 1.7 (see Figure 5 of Sapozhnikov and Foufoula-Georgiou [1997]). This value of  $D$  relates to  $\nu_x$  and  $\nu_y$  by the expression [see Sapozhnikov and Foufoula-Georgiou, 1995]

$$D_G \equiv D = (\nu_y - \nu_x + 1)/\nu_y. \quad (22)$$

Combining the above equation with (3), (20), and (21) results in

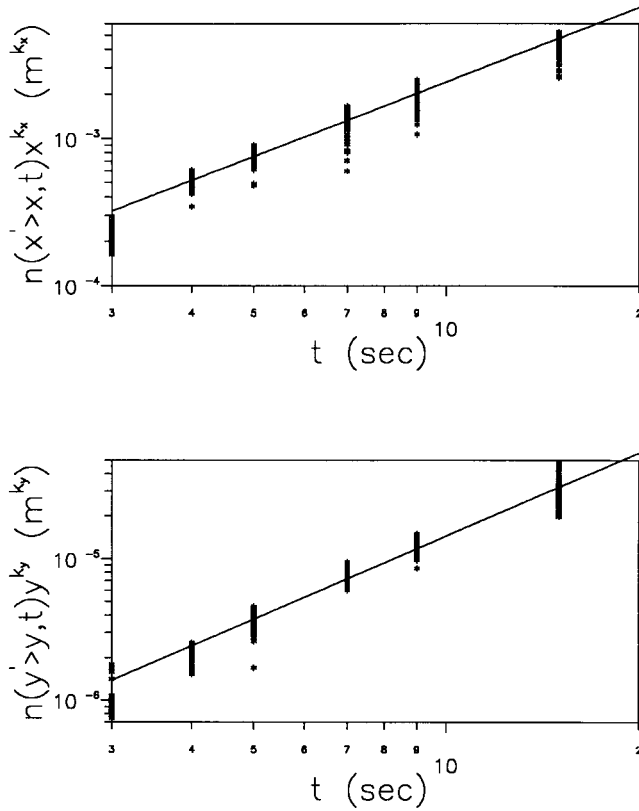


**Figure 2.** Evolution of the distribution of changes shown by the time dependence of the functions  $n(x' > x, t)x^{k_x}$  and  $n(y' > y, t)y^{k_y}$  for the X and Y directions, respectively. For every time lag, each point on the plots shows the (rescaled by  $x^{k_x}$  or  $y^{k_y}$ ) number of changes exceeding size  $x$  or  $y$ , respectively. The plots suggest that power law dependence applies in both directions well over a major part of the range.

$$\nu_x = \frac{k_y\beta_x + (\beta_y - \beta_x)(D - 1)}{k_x\beta_y(D - 1) + k_y\beta_x} \quad (23)$$

$$\nu_x = \frac{\beta_x - \beta_y + k_x\beta_y}{k_x\beta_y(D - 1) + k_y\beta_x} \quad (24)$$

The above equations enabled us to estimate indirectly the fractal exponents of the experimental river as  $\nu_x = 0.61$  and  $\nu_y = 0.55$ . Finally, from (20) and (21) we found the dynamic exponents of the braided river as  $z_x = 0.32$  and  $z_y = 0.35$ . Thus it was concluded that the experimental river exhibits anisotropic dynamic scaling with anisotropy ratio  $z_y/z_x = \nu_x/\nu_y = 1.1$ .

It is important to note that although for small time lags Figure 2 shows reasonably good temporal scaling, it deviates from the power law behavior for bigger time lags (i.e., for time lags  $t > 15$  s not shown in Figure 2). It should be stressed however, that this does not indicate the loss of dynamic scaling expressed by the general equations for dynamic scaling (12) and (13). In fact, even though the functions  $f_x$  and  $f_y$ , from (12) and (13), follow power laws at small values of the argument, they have to level off at big values of the argument. Indeed, for big enough time lags such that the object decorrelates completely between the snapshots, the difference between the two patterns of the object (and therefore the distribution of changes  $n(x' > x, t)$  and  $n(y' > y, t)$ ) does not depend on

time anymore. This necessarily leads to the loss of power law dependencies in relations (16) and (17) but not loss of dynamic scaling. In fact, to confirm that the distributions corresponding to different time lags satisfy the general equations for dynamic scaling (12) and (13), we plotted for the estimated values of  $\nu_x$ ,  $\nu_y$ ,  $z_x$ , and  $z_y$ , the values of  $n(x' > x, t)x^{-1/\nu_x}$  versus  $t/x^{z_x}$ , and  $n(y' > y, t)y^{-1/\nu_y}$  versus  $t/y^{z_y}$ , for different time lags up to 1 min, in Figure 3. As one can see, in both cases all curves satisfactorily collapse to a single curve (the  $f_x(t/x^{z_x})$  and  $f_y(t/y^{z_y})$  curve, respectively).

This further corroborates the presence of dynamic scaling and the adequacy of the estimated dynamic exponents  $z_x = 0.32$  and  $z_y = 0.35$  in the experimental braided river. Notice that this last confirmation of dynamic scaling, i.e., that the general equations for dynamic scaling (12) and (13) hold, did not directly use the assumption of power-law distribution of changes (equations (14) and (15)) or power law dependence of  $\psi_x(t)$  and  $\psi_y(t)$  for small values of  $t$  (equations (16) and (17)). These two special forms of dependencies (suggested directly from the experimental data in Figures 1 and 2) were conveniently used only to estimate  $z_x$  and  $z_y$  in a stepwise manner via equations (20) and (21). After the values of  $z_x$  and  $z_y$  were estimated, plotting  $n(x' > x, t)x^{-1/\nu_x}$  versus  $t/x^{z_x}$  and  $n(y' > y, t)y^{-1/\nu_y}$  versus  $t/y^{z_y}$ , and seeing that in each case all curves collapse to one, the  $f_x$  or  $f_y$  curve respectively, provides an additional and independent evidence for anisotropic dynamic scaling.

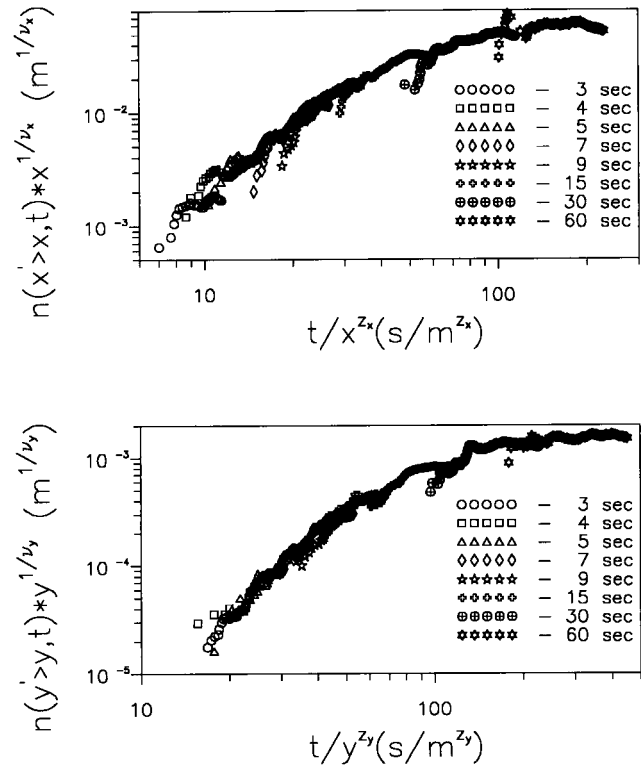


**Figure 3.** Plot showing that the rescaled distributions of changes collapse into a single curve,  $f_x$  and  $f_y$ , for each direction X and Y, respectively. Time lags from 3 to 60 s (bottom left to top right) are shown in each plot. This further corroborates the presence of anisotropic dynamic scaling and the adequacy of the estimated values of  $z_x$  and  $z_y$ .

#### 4. Discussion and Conclusions

In a previous study by Sapozhnikov and Foufoula-Georgiou [1997], evidence was presented that braided rivers exhibit dynamic scaling with scaling exponent  $z \approx 0.5$ . In that study, braided rivers were analyzed as self-similar objects despite the existing evidence that they exhibit spatial scaling anisotropy, i.e., that they are self-affine objects [Sapozhnikov and Foufoula-Georgiou, 1996]. The reason for exploring dynamic scaling in braided rivers within the self-similarity framework first, was that developing the corresponding theory was easier conceptually in that case and its extension to self-affinity was not trivial. The results were interpreted considering  $D$  (the fractal dimension of a self-similar object) as a surrogate parameter for  $D_G$  (the global fractal dimension of a self-affine object) which relates to  $\nu_x$  and  $\nu_y$  via (22).

In this paper, the theoretical framework for describing dynamic scaling was extended to self-affine objects and was applied to the same experimental braided river data as in Sapozhnikov and Foufoula-Georgiou [1997]. The results indicated the presence of anisotropic dynamic scaling in braided rivers and gave us estimates of the dynamic exponents  $z_x = 0.32$  and  $z_y = 0.35$ . The approach presented in this paper is more general than the one by Sapozhnikov and Foufoula-Georgiou [1997] as it is capable of taking into account the self-affinity of the analyzed object. At the same time, it can also be used for the analysis of self-similar objects as a special case. We consider this approach more consistent for the analysis of braided rivers and believe that it is the values of  $z_x$  and  $z_y$  (rather than the single value of  $z$ ) that really characterize the dynamic scaling in braided rivers.

The physical interpretation of the dynamic exponent  $z$  was extensively discussed by Sapozhnikov and Foufoula-Georgiou [1997] and was interpreted as an indication that evolution of small channel patterns is to a large extent forced by the evolution of larger channels. The exact same interpretation applies here for the  $z_x$  and  $z_y$  values, each one associated with the evolution of channels along the slope and in perpendicular direction, respectively.

It should be noted that in the experimental river, the estimated scaling anisotropy parameter  $\nu_x/\nu_y = 1.1$  is considerably lower than the value of 1.4 to 1.5 estimated for natural rivers using the LCI method. It remains to be determined whether this discrepancy reflects differences in the spatial structure of natural versus laboratory produced rivers or is due to the differences in the estimation methods (one based on the static images only versus the other based on system dynamics). It is emphasized that in this work the fractal exponents  $\nu_x$  and  $\nu_y$  were not explicitly estimated from the braided river pattern as was done for natural rivers. Rather they were estimated implicitly from the analysis of changes. Thus the developed approach enables one to estimate the values of the fractal exponents of the spatial structure of a braided river from the dynamics of the river. As such, it takes advantage of the data collected during some time interval, rather than relying on the analysis of one snapshot only using, for example the LCI method. The two estimation methods should be compared to each other so that the properties of their estimates of  $\nu_x$  and  $\nu_y$  can be better understood. Such a comparison was not possible with the experimental data used in this study since, as was discussed, the dye procedure did not allow for many scales to

be resolved in the static patterns, as needed for the LCI method. Different techniques giving higher-resolution experimental data or remote sensing images of natural braided rivers might permit such a comparison in the near future.

As a closing remark, it is noted that the presence of spatial and dynamic scaling was interpreted by Sapozhnikov and Foufoula-Georgiou [1997] as indication of self-organized criticality (SOC) in braided rivers. In view of the results of this article where anisotropic dynamic scaling was established, braided rivers are further interpreted as SOC systems showing spatio-temporal anisotropy in the critical state. To our knowledge, this type of behavior has never been found in classical systems i.e., systems brought to a critical state not by self-organization, but by tuning of a critical parameter (e.g., temperature). Thus a general problem that remains open to investigation is the development of theoretical frameworks for the description of the critical state of self-affine objects.

**Acknowledgments.** This research was supported by NSF grant EAR-9628393 and NASA grant NAG5-6191. Supercomputer resources were kindly provided by the Minnesota Supercomputer Institute.

#### References

- Ashmore, P. E., Laboratory modelling of gravel braided stream morphology, *Earth Surf. Proc. Landforms*, 7, 201–225, 1982.
- Ashmore, P. E., How do gravel-bed rivers braid?, *Can. J. Earth Sci.*, 28, 326–341, 1991.
- Barzini, G. N., and R. C. Ball, Landscape evolution in flood—A mathematical model, *J. Phys. A Math. Gen.*, 26, 6777–6787, 1993.
- Howard, A. D., M. E. Keetch, and C. L. Vincent, Topological and geometrical properties of braided streams, *Water Resour. Res.*, 6, 1674–1688, 1970.
- Kuhnle, R. A., An experimental study of braiding in gravel-bed streams, M.S. thesis, Univ. Illinois, Chicago, 1981.
- Leddy, J. O., P. J. Ashworth, and J. L. Best, Mechanisms of anabranch avulsion within gravel-bed braided rivers: Observations from a scaled physical model, in *Braided Rivers*, edited by J. L. Best and C. S. Bristow, pp. 119–127, Geol. Soc. of London, London, 1993.
- Murray, A. B., and C. Paola, A cellular automata model of braided rivers, *Nature*, 371, 54–57, 1994.
- Sapozhnikov, V., and E. Fofoula-Georgiou, Study of self-similar and self-affine objects using logarithmic correlation integral, *J. Phys., A Math. Gen.*, 28, 559–571, 1995.
- Sapozhnikov, V., and E. Fofoula-Georgiou, Self-affinity in braided rivers, *Water Resour. Res.*, 32, 1429–1439, 1996.
- Sapozhnikov, V. B., and E. Fofoula-Georgiou, Experimental evidence of dynamic scaling and indications of self-organized criticality in braided rivers, *Water Resour. Res.*, 33, 1983–1991, 1997.
- Schumm, S. A., and H. R. Khan, Experimental study of channel patterns, *Geol. Soc. Am. Bull.*, 83, 1755–1770, 1972.
- Smith, L. C., B. L. Isacks, R. R. Forster, A. L. Bloom, and I. Preuss, Estimation of discharge from braided glacial rivers using ERS 1 synthetic aperture radar: First results, *Water Resour. Res.*, 31, 1325–1329, 1995.
- Smith, L. C., B. L. Isacks, A. L. Bloom, and A. B. Murray, Estimation of discharge from three braided rivers using synthetic aperture radar satellite imagery: Potential application to ungaged basins, *Water Resour. Res.*, 32, 2031–2034, 1996.

E. Fofoula-Georgiou and V. B. Sapozhnikov, St. Anthony Falls Laboratory, University of Minnesota, Mississippi River at Third Avenue, SE, Minneapolis, MN 55414-2196. (efi@mykonos.safhl.umn.edu)

(Received November 18, 1997; revised January 12, 1998; accepted January 14, 1998.)

